# CHARACTERIZATION OF FIBROUS REINFORCEMENTS BY CAPILLARY FLOW POROMETRY: INFLUENCE OF FIBER VOLUME FRACTION

Bonnard, B, Causse, P, and Trochu, F*
Department of Mechanical Engineering, Polytechnique Montreal, Canada
* Corresponding author (trochu@polymtl.ca)

**Keywords***: Capillary flow porometry, dual scale porosity, fibrous reinforcement*

## ABSTRACT

*Liquid Composite Molding* (LCM) processes involve an injection stage during which a liquid reactive resin is forced into a dry fibrous preform. This manufacturing step is crucial to reach full impregnation and produce high performance composites. However, the resin flow is a complex process since textile reinforcements consist of an arrangement of fiber bundles that exhibit a dual scale porosity. Microscopic elongated voids called micropores are present between the fibers inside the tows while much larger empty spaces called mesopores exist between the textile yarns. Previous work showed that *Capillary Flow Porometry* (CFP) is a promising technique to measure the size of microscopic and mesoscopic pores [1]. This method is based on liquid expulsion by applying an increasing air pressure to one edge of a fully wetted specimen of the fibrous reinforcement. Assuming a cylindrical pore model, the air flow through the wet and dry sample necessary to expel the liquid is measured to estimate the pore size distribution. The present study based on this approach aims to investigate the influence of compaction on the dual-scale porosity of engineering textiles commonly used in composites. A new experimental setup was devised to control the compression state of the tested sample. This device was used to conduct through-thickness porometry measurements with varying fiber volume fractions. For all the materials studied, the experimental results confirm, as expected, that the average diameter of the micropores and mesopores decreases when the fiber volume fraction increases. Hence, CFP can be used to evaluate quantitatively the influence of compaction on the pore size distribution. Such information is highly valuable to better understand dual-scale flows in fibrous reinforcements together with their impact on void formation and transport. This methodology can improve in the future the robustness of LCM processes to fabricate high quality composites by resin injection.

## 1 INTRODUCTION

During *Liquid Composite Molding* (LCM) processes, a preform consisting of a stack of dry fibrous reinforcements is impregnated by a polymeric resin. Achieving a high level of saturation of the porous preform is critical due to the dual-scale porosity of the fibrous structure. Indeed, fibers are gathered at the microscopic scale to form bundles and the bundles are woven or stitched together to form a fabric, so that volumes of mesoscopic scale are present in between the bundles. Due to the difference in the scale of the pores, the flow is driven by two competitive forces : viscous forces in the mesopores and capillary forces in the micropores [2]. This results in varying resin velocities at the flow front that can cause void formation through mechanical air entrapment [3, 4]. Consequently, characterizing the porous structure of the fiber beds can be of great help to understand resin flow and develop modeling tools. For example, Vernet and Trochu [5, 6] used microscopy to analyze serial cuts in composite parts and measured the pore size distribution between fiber tows to predict the permeability of 3D interlock fabrics. Schell et al. used a similar approach to determine the average distance between fibers and computed the capillary pressure inside fiber tows that was subsequently used in a numerical model predicting void creation during filling [4]. Fibrous reinforcements can also be characterized using advanced experimental techniques based on X-ray microtomography. Straumit et al. [7] used this technique to reconstruct the morphology of mesopores in composites to predict the permeability of the reinforcing textile. X-ray tomography can also give detailed

observations at the microscopic scale as shown by Latil et al. [8], who studied the evolution of fiber bundle porosity during transverse compaction.
The potential of *Capillary Flow Porometry* (CFP) was investigated previously to characterize the fibrous reinforcements used in composite materials [1, 9]. The method consists of expelling a completely wetting liquid from a saturated sample with an increasing air pressure in order to assess the pore size distribution. This approach appears promising because of its simplicity and the capability to characterize the dual scale porosity in a repeatable way. However, the testing procedure used in past investigations did not reproduce perfectly real manufacturing conditions since the compaction state of the sample was not strictly controlled. The objective of this study is to improve the experimental methodology and analyze the impact of fabric compaction on the pore size distribution measured by CFP. It is indeed well-known that the fiber volume fraction has a major influence on resin impregnation during composite manufacturing in rigid molds [10-13]. The paper is divided into two main sections. Firstly, the device used for the measurements, the experimental CFP test procedure and associated data processing are presented. The second part details the results obtained with a typical glass woven reinforcement for different fiber volume fractions.

# 2 MATERIALS AND METHODS

## *2.1 Material tested*

All the experiments presented in this study were carried out with a 3x2 double twill weave reinforcement from Texonic (product ID L1402197). The textile architecture is illustrated in Figure 1. This fabric is made of E glass fiber bundles and possesses an areal density of 1024 g/m$^2$. The fabric ply thickness (1.27 mm) was measured according to the ASTM D1777 [14] and corresponds to a natural fiber volume fraction of 31%.

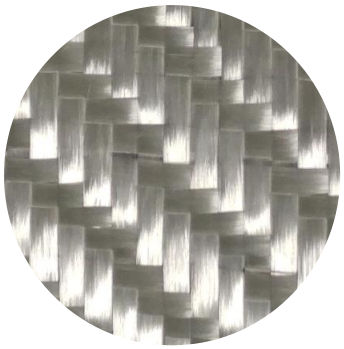

Figure 1. Top view of the glass twill weave reinforcement L1402197.

## *2.2 Apparatus and experimental setup*

CFP measurements were performed with a 3Gz Porometer from Quantachrome Intruments Inc. This apparatus can originally receive different sample holders depending on the sample size and the measurement direction. This device is usually employed to characterize nearly incompressible materials and the existing sample holders do not allow control of the compaction state. Consequently, a new setup for through-thickness measurement was devised based on an existing cylindrical sample holder. The complete assembly is shown in Figure 2. The porous sample is placed between two perforated rigid grids and calibrated shims are used to adjust the overall thickness of the cavity. The top support grid is glued to the sample container bottom to facilitate handling of the sample. All the inserts and shims are removable and can be manipulated outside the sample holder. The tested sample has a diameter of 32 mm and maximum thickness of 6 mm.

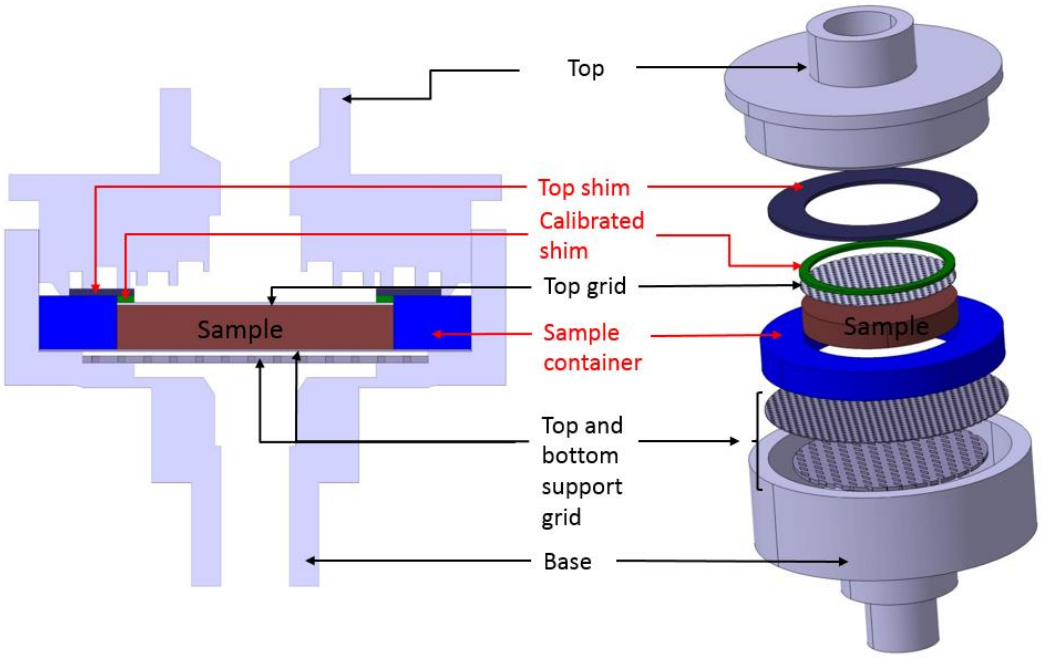


Figure 2. New sample holder for through-thickness porometry measurements with controlled fiber volume fraction.

### *2.3 Test methodology*

Specimens of diameter 32 mm were cut from the fabric roll with a custom-made punch actioned by a hydraulic press. With careful manipulation, three plies of reinforcement were placed on the top support grid in the sample container. The plies were positioned in the same direction. A porous grid as well as shims of adequate thicknesses were placed on top of the sample. The whole sample container, including the grids and the shims, was then immersed in a Petri dish containing a completely wetting liquid called Porofil®. This fluid is a proprietary perfluorinated compound recommended by Quantachrome because of its null contact angle with nearly all kind of solids. It also exhibits a low vapor pressure, a medium viscosity (approximatively 2-3 mPa.s at 20°C) and a low surface tension (0.016 N/m). To ensure a maximum saturation of the porous media by the wetting liquid, the Petri dish with the sample container was degassed twice in a vacuum bell for two minutes. Before applying vacuum, a few drops of Porofil® were poured on top of the sample. The sample container was then placed inside the sample holder and the assembly was manually closed before launching the experiment. As shown in Figure 2, closing the assembly implies contact between the top shim and the sample container. The perforated grids are assumed to be perfectly rigid so that the fiber fraction of the sample remains constant as determined by the thickness of the calibrated shims. However, note that a verification procedure is currently being developed to test this hypothesis. The test sequence is divided in two main steps that are completely controlled by the software 3Gwin V2.2. During each step, a controlled air pressure is progressively applied on top of the specimen and the flow rate passing through the sample is recorded.

Typical experimental results showing the air flow rate as a function of the imposed pressure are reported in Figure 3. At the beginning of the first ramp, called the wet run, air cannot pass through the sample since the pressure is too low to expel the wetting liquid from the pores. When the pressure becomes high enough, the largest pore is emptied and a first positive value of flow rate is detected. This position is commonly referred to as the bubble point, which corresponds to the largest pore in the specimen. Then, the liquid is progressively expelled and the flow passing through the sample increases stepwise. At the end of the wet run, the sample should normally be completely drained and a second ramp called the dry run is conducted involving the same pressure range. As illustrated in Figure 3, the first intersection between the wet and dry curves corresponds to the smallest pore

detected in the sample. After this point, the two curves are superposed, which confirms that the maximum applied pressure is sufficient to empty all the pores during the wet run.

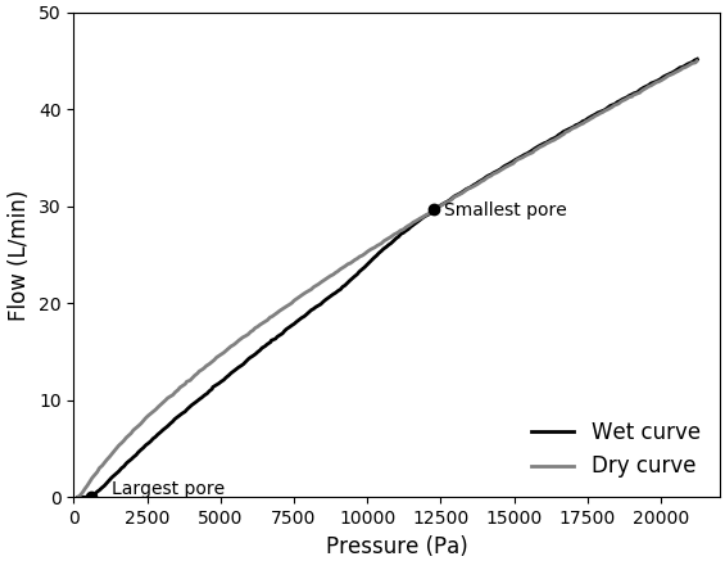


Figure 3. Typical results obtained by CFP measurement (test at $V_f$ = 63%).

### *2.4 Data processing*

The analysis of experimental data was performed with an improved version of the Python code presented previously [9]. Raw data of a typical measurement consists of 256 measurement points corresponding to the flow passing through the sample as a function of the air pressure applied during the run. The wet and dry curves were first interpolated by kriging, a statistical interpolation method, to obtain two mathematical functions describing the relationship between flow rate and applied pressure. As illustrated in Figure 4, the kriged functions give a good representation of the observed behavior. Note also that the kriged curves do not necessarily pass by the measurement points, because a nugget effect is used to account for the measurement errors induced by sensor noise. As compared to previous work, new parameters were added to the kriging function to improve the accuracy of the interpolation. Firstly, a constraint was considered at the beginning of the wet curve to set the derivative to zero before the bubble point. This helped to obtain a better accuracy on the largest pore size. Then, the nugget effect was chosen as a variable parameter proportional to the flow rate value. The goal here is to reflect the actual sensor measurement error.

Two types of cumulative flow distributions were obtained by dividing the wet kriged function by the dry one. The first cumulative curve shown in Figure 5a gives the relative percentage of the overall flow as a function of pore pressure. For the selected example, approximately 80% of the overall flow passes through pores for a pressure lower than 5000 Pa. The second curve represents the cumulative flow as a function of the pore diameter (Figure 5b). To obtain the equivalent pore diameter corresponding to pore pressure, it is assumed that the fibrous reinforcement consists of a network of parallel cylindrical pores. The pore diameter is then calculated by Young-Laplace equation:

$$D = \frac{4\gamma \cos\theta}{P} \tag{1}$$

where $\gamma$ is liquid surface tension, $\theta$ is the contact angle of the liquid and $P$ is the applied pressure. As mentioned before, the Porofil® has a contact angle nearly equal to zero so that this equation can be simplified by setting $\cos\theta = 1$. Note that this assumption on pore geometry does not actually reflect the complex structure of fibrous reinforcements. However, this approach provides an effective way to measure the pore size distribution, hence allowing a quantitative comparison between different experiments.

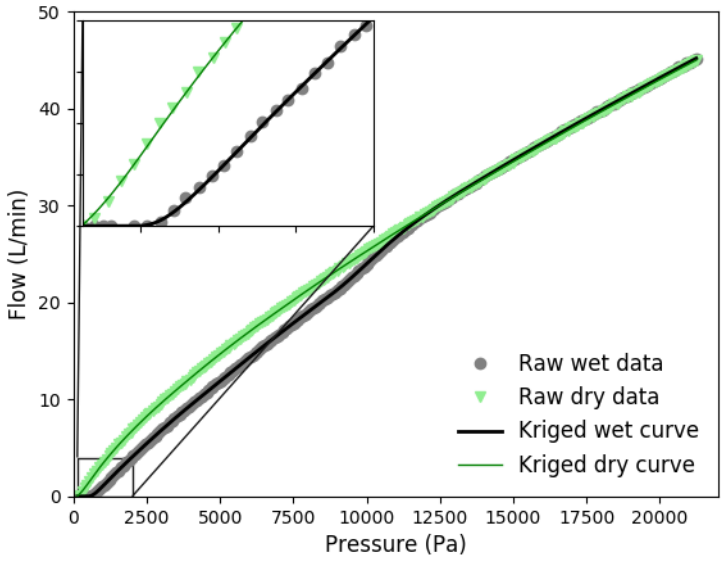


Figure 4. Dual kriging smoothing function applied to the raw wet and dry data (test at $V_f$ = 63%).

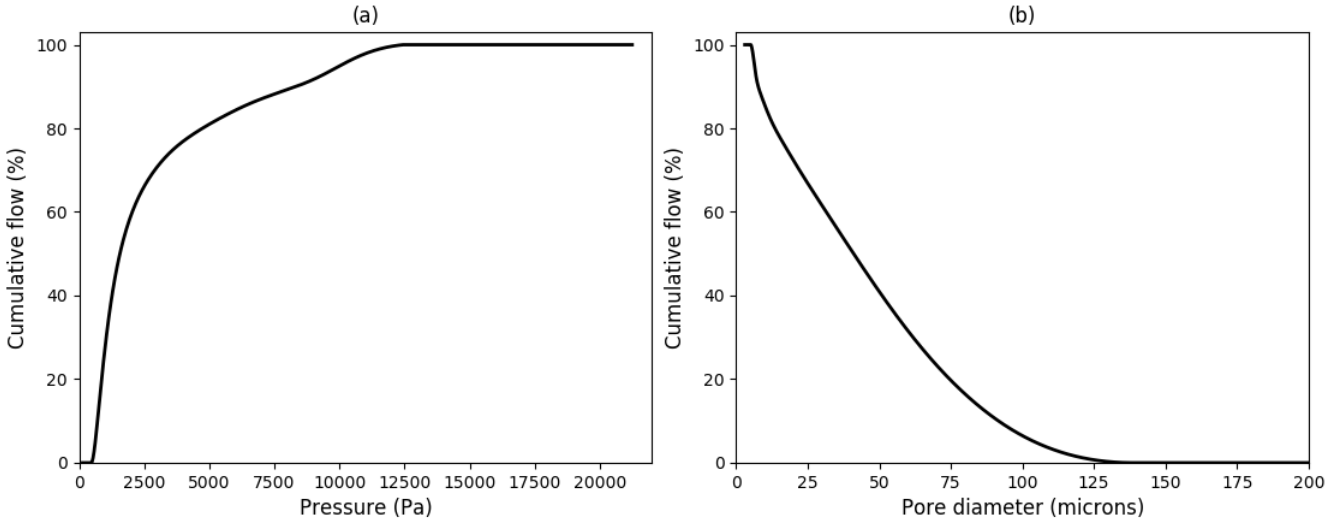


Figure 5. Typical cumulative flow curves: (a) as a function of pressure; (b) as a function of pore diameter (test at $V_f$ = 63%).

Finally, the cumulative curves were derived numerically to obtain two differential flows. The differential flow as a function of pore pressure is shown in Figure 6a. Each point on this curve represents the percentage of flow passing through a pressure range of one Pascal (nominal value ± 0.5 Pa). This curve exhibits a large peak in the

lower pressure range that can be associated with mesopores. A smaller peak is also visible on the opposite side of the distribution, which reflects the presence of micropores. On the other hand, the differential flow as a function of pore diameter is shown in Figure 6b, which represents the percentage of flow passing through a pore size range of one micron (nominal value ± 0.5 µm). In porometry, this curve is usually referred to as the pore size distribution. In this case, a sharp peak is associated with the micropores. The presence of mesopores can also be identified, although it is more difficult to associate them with a clearly defined peak.

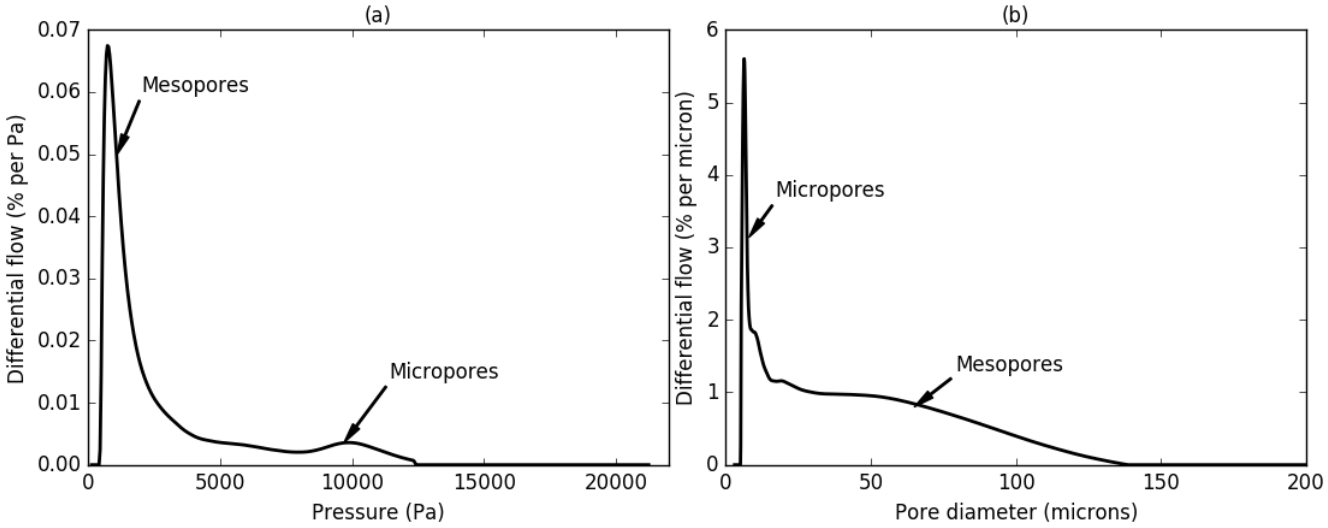


Figure 6. Typical differential flow curves: (a) as a function of pressure, showing mainly a peak of mesopores; (b) as a function of pore diameter, showing a peak in micropores (test at $V_f$ = 63%).

# 3 RESULTS AND DISCUSSION

## *3.1 Repeatability of the measurements*

A series of preliminary tests were conducted on the same fabric sample to evaluate the repeatability of the experimental procedure without considering the effect of the intrinsic material variability. The first tests were carried out at a fiber volume fraction of 37%, and then the calibrated shims were changed gradually to increase the fiber fraction to 46, 57 and 63%. The measurements were repeated three times for each fiber content. Typical results are reported in Figure 7 for a volume fraction of 57%. As shown in in this figure, small variations (below 10%) exist between the overall wet and dry curves for different tests. However, the effect of these differences on the corresponding pore size distribution remains minor (see Figure 7b). For example, the repeatability of the location and intensity of the micropore peak is quite satisfactory. Similar results (not reported here) were obtained for the mesopore peak of the pore pressure distribution.

The influence of sample-to-sample variations was then evaluated by testing four different fabric samples. Each specimen was tested once at the fiber volume fraction considered previously. Note that the tests were always conducted in ascending order of fiber content to avoid possible permanent deformations resulting of compaction. Figure 8a shows the flow rates curves obtained at a fiber volume fraction of 57%. (Similar results were obtained for the other fiber volume fractions considered.) As reported, the general shape of the wet and dry curves is very similar. The maximum difference in the overall flow between two experiments is close to 15%. This kind of variations was rather expected since it accounts not only for the variability of the fibrous material, but also for the experimental errors of the testing procedure. The corresponding pore size distributions shown in Figure 8b are

very close to one another. It is notably very interesting to point out that the position and intensity of the micropore peak can be precisely determined in a reproducible way (see zoomed panel in Figure 8b). Note also that a similar conclusion can be drawn on the mesopore peak from the pore pressure distribution (not reported here). Overall, the repeatability of CFP measurements is quite satisfactory, which confirms the robustness of this approach to characterize dual-scale porous media such as the fibrous reinforcement considered here.

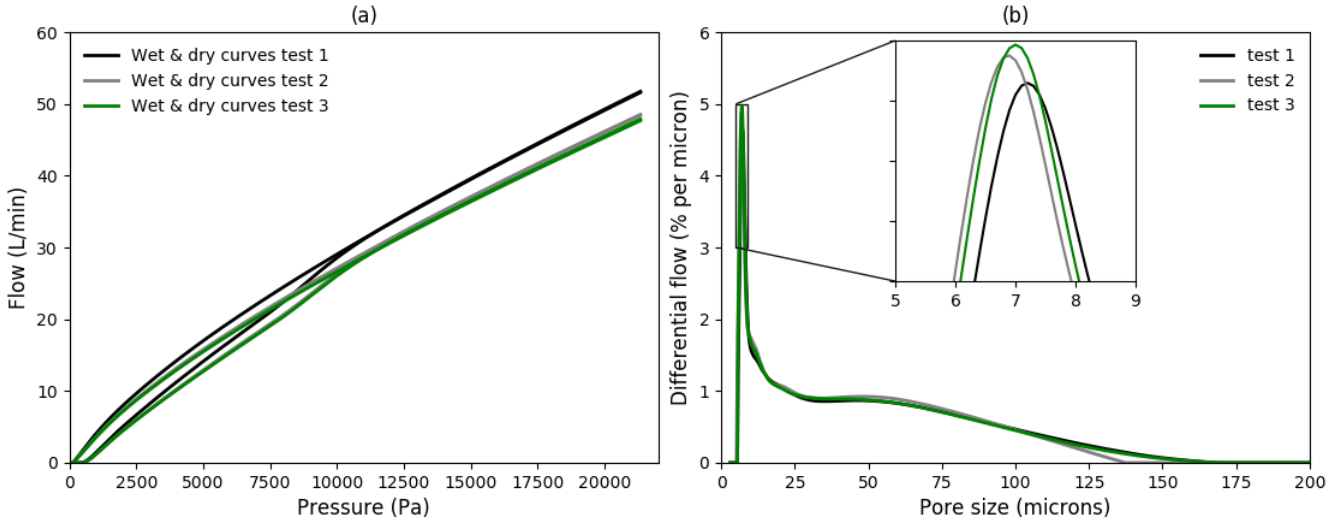


Figure 7. Repeatability of the measurement on the same fabric sample at a fiber volume fraction of 57%.

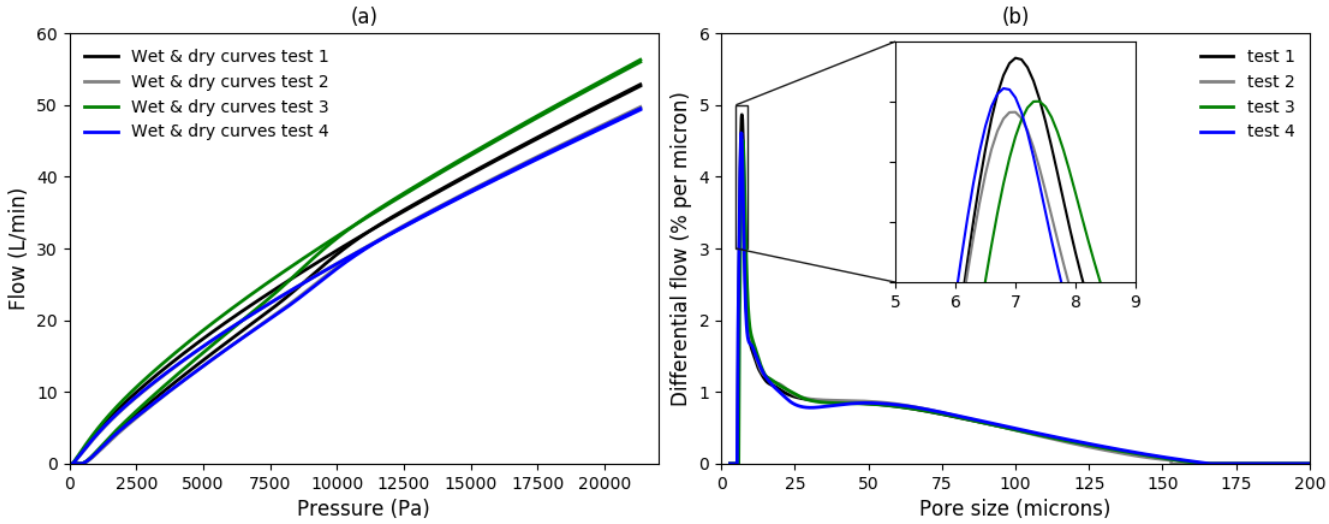


Figure 8. Repeatability of measurements for four different samples at a fiber volume fraction of 57%.

### *3.2 Influence of fiber volume fraction*

Figure 9 shows the mean pore size distributions obtained by averaging results from CFP measurements on four different samples. Firstly, these curves approximately cross each other around a diameter of 100 µm. For the lowest fiber fraction (37%), a significant flow passes through larger pores. When the fiber fraction increases, this

part of the distribution flattens considerably and almost no flow is detected is this range of diameter for a fiber fraction of 63%. On the other hand, the overall amount of flow recorded in the range 20-100 µm increases with the fiber volume fraction. This suggests that compaction reduces the size of the largest pores, but that still significant flow channels remain at the mesoscale in highly compacted samples. The reorganization of the empty space between the bundles is also illustrated in Figure 10, which plots the largest pore detected and the location of the mesopore peak (from the pore pressure distribution curve). These two parameters follow the same trend when the compaction of the fabric increases. The influence of the fiber fraction on the mesopores seems to be more important when $V_f$ is lower than 45%. For higher compaction levels, the evolution of the respective diameters appears to be linear. However, note that the data gathered remains limited and that additional experiments are required to confirm this analysis. Figure 9 also shows that compacting the fabric affects the porosity at the microscopic scale within fiber bundles. When the fiber volume fraction is increased, the micropore peak intensity increases (from 2.5 to 5.4 %/µm) and its position is shifted towards lower diameters. As reported in Figure 11, the equivalent diameter of the peak varies almost linearly and is reduced by 35% when the fiber volume fraction increases from 37% to 63%. A similar trend is observed for the smallest pores detected, which decrease from 8.4 to 5.1 µm.

Overall, the above results show that compaction of the fabric generates a reorganization of the porous medium at both the microscopic and mesoscopic scales. However, note that CFP measures only the pore size in the most restricted section along the air pathway. Further investigation is still needed to verify if the influence of compaction on the pore size distribution measured by CFP is representative of the entire porous structure in an averaged sense. To reach that goal, porometry could be compared with other characterization techniques such as X-ray microtomography for example.

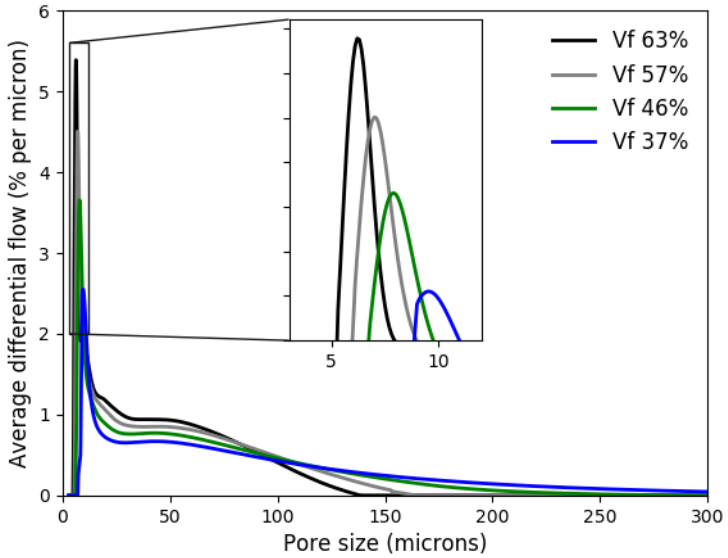


Figure 9. Influence of fiber volume fraction on the mean pore size distribution.

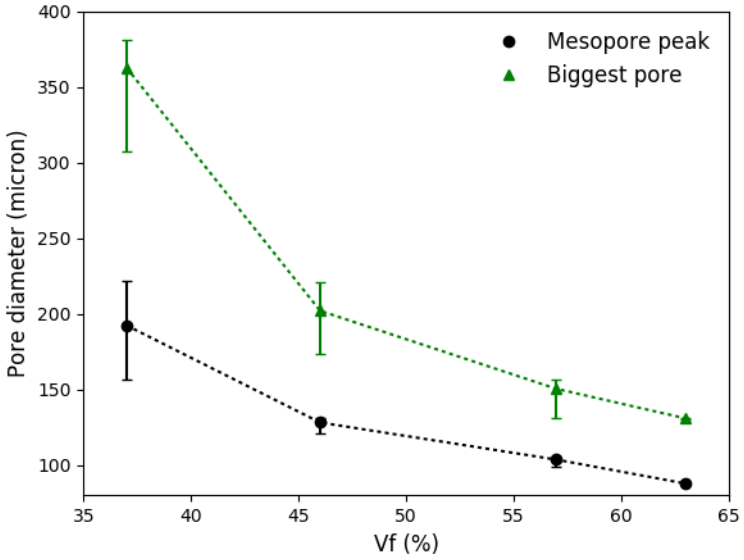


Figure 10. Influence of fiber volume fraction on the mesopore peak and on the largest pore (error bars indicate the minimum and maximum values of 4 repeated tests).

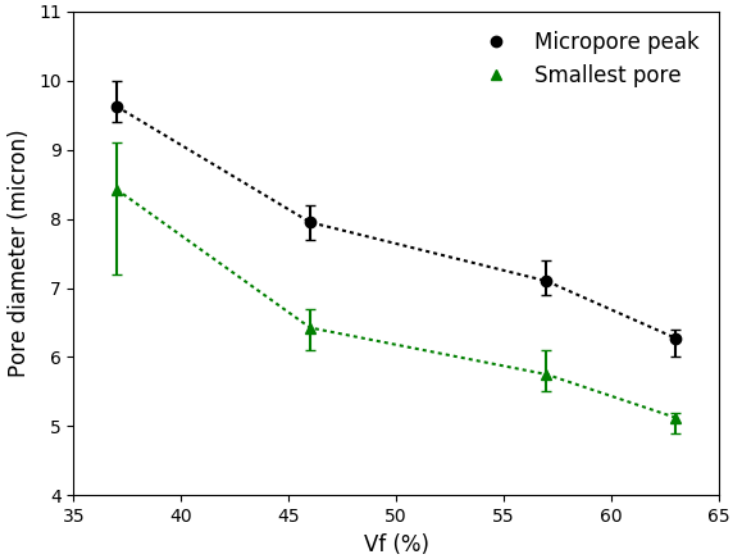


Figure 11. Influence of fiber volume fraction on the micropore peak and on the smallest pore (error bars indicate the minimum and maximum values of 4 repeated tests).

# 4 CONCLUSION

This work investigated the influence of fiber volume fraction on the pore size distribution in engineering textiles based on a new experimental methodology known as *Capillary Flow Porometry*. The study was conducted using a commercial porometer equipped with a specially devised sample holder. This new device allows controlling the level of compaction of the sample during the porometry test. The processing of experimental data was also improved to detect automatically the smallest and largest pores as well as the diameters associated with the differential flows in micropores and mesopores. The methodology was applied to characterize a glass woven reinforcement in a range of fiber volume fractions typically used in *Liquid Composite Molding*. The results show that both micropores and mesopores sizes decrease when the fabric is compacted. Moreover, CFP allows quantifying the relative amount of flow associated with different pore sizes. Such information could be valuable to better understand the flow mechanisms in dual-scale porous media and in the end, improve the quality of composites made by resin injection.

# 5 REFERENCES

[1] B. Bonnard, P. Causse, and F. Trochu. "Experimental Investigation of Capillary Flow Porometry for Characterization of Fibrous Reinforcements in Composite Materials". *13th Int. Conf. on Flow Pro. in Comp. Mat. (FPCM13)*, Kyoto, Japan, 2016.

[2] F. LeBel, A. E. Fanaei, E. Ruiz, and F. Trochu. "Prediction of optimal flow front velocity to minimize void formation in dual scale fibrous reinforcements". *International Journal of Material Forming*, Vol. 7, No. 1, pp 93-116, 2014.

[3] M. K. Kang, W. I. Lee, and H. T. Hahn. "Formation of microvoids during resin-transfer molding process". *Composites Science and Technology*, Vol. 60, No. 12–13, pp 2427-2434, 2000.

[4] J. S. U. Schell, M. Deleglise, C. Binetruy, P. Krawczak, and P. Ermanni. "Numerical prediction and experimental characterisation of meso-scale-voids in liquid composite moulding". *Composites Part A: Applied Science and Manufacturing*, Vol. 38, No. 12, pp 2460-2470, 2007.

[5] N. Vernet and F. Trochu. "Analysis of mesoscopic pore size in 3D-interlock fabrics and validation of a predictive permeability model". *Journal of Reinforced Plastics and Composites*, Vol. 35, No. 6, pp 471-486, 2016.

[6] N. Vernet and F. Trochu. "In-plane and through-thickness permeability models for three-dimensional Interlock fabrics". *Journal of Composite Materials*, Vol. 50, No. 14, pp 1951-1969, 2015.

[7] I. Straumit, C. Hahn, E. Winterstein, B. Plank, S. V. Lomov, and M. Wevers. "Computation of permeability of a non-crimp carbon textile reinforcement based on X-ray computed tomography images". *Composites Part A: Applied Science and Manufacturing*, Vol. 81, pp 289-95, 2016.

[8] P. Latil, L. Orgeas, C. Geindreau, P. J. J. Dumont, and S. Rolland du Roscoat. "Towards the 3D in situ characterisation of deformation micro-mechanisms within a compressed bundle of fibres". *Composites Science and Technology*, Vol. 71, No. 4, pp 480-488, 2011.

[9] B. Bonnard, P. Causse, and F. Trochu. "Experimental characterization of the pore size distribution in fibrous reinforcements of composite materials". *Journal of Composite Materials*, doi:10.1177/0021998317694424, 2017.

[10] E. Rodriguez, F. Giacomelli, and A. Vazquez. "Permeability-porosity relationship in RTM for different fiberglass and natural reinforcements". *Journal of Composite Materials*, Vol. 38, No. 3, pp 259-268, 2004.

[11] C.-H. Shih and L. J. Lee. "Effect of fiber architecture on permeability in liquid composite molding". *Polymer Composites*, Vol. 19, No. 5, pp 626-639, 1998.

[12] C. Di Fratta, F. Klunker, F. Trochu, and P. Ermanni. "Characterization of textile permeability as a function of fiber volume content with a single unidirectional injection experiment". *Composites Part A: Applied Science and Manufacturing*, Vol. 77, pp 238-247, 2015.

[13] H. C. Stadtfeld, M. Erninger, S. Bickerton, and S. G. Advani. "An experimental method to continuously measure permeability of fiber preforms as a function of fiber volume fraction". *Journal of Reinforced Plastics and Composites*, Vol. 21, No. 10, pp 879-899, 2002.

[14] Y. S. Song, K. Chung, T. J. Kang, and J. R. Youn. "Prediction of permeability tensor for three dimensional circular braided preform by applying a finite volume method to a unit cell". *Composites Science and Technology*, Vol. 64, No. 10-11, pp 1629-1636, 2004.